2012 IEEE International Conference on Robotics and Automation
RiverCentre, Saint Paul, Minnesota, USA
May 14-18, 2012

Towards a Compact Robotically Steerable Thermal Ablation Probe

Carmen M. Graves, Alex Slocum, Rajiv Gupta, and Conor J. Walsh, *Member, IEEE*

Abstract— **The focus of this paper is on the design and evaluation of a robust drive mechanism intended to robotically steer a thermal ablation electrode or similar percutaneous instrument. We present the design of an improved screw-spline drive mechanism based on a profiled threaded shaft and nut that reduces the part count and simplifies manufacturing and assembly. To determine the optimal parameters for the profile shape, an analytical expression was derived that relates the tolerance between the nut and shaft to the angular backlash, which was validated using SolidWorks. We outline the forward kinematics of a steering mechanism that is based on the concept of substantially straightening a pre-curved Nitinol stylet by retracting it into a concentric outer cannula, and re-deploying it at a different position. This model was compared to data collected during targeting experiments performed in ex-vivo tissue samples where the distal tip of the stylet was repositioned in ex-vivo bovine tissue and the location of its distal tip was recorded with CT imaging. Results demonstrated that the drive mechanism operated robustly and targeting errors of less than 2mm were achieved.**

I. Introduction

An increasing number of minimally invasive surgeries have begun to replace traditionally open procedures since the last quarter of the 20th century. Not only does minimally invasive surgery reduce the trauma to the patient by decreasing pain, risk of infection, and scarring, but it also greatly reduces the cost of the procedure for the hospital due to shorter stays.

More recently, robotics has begun to take a greater role in minimally invasive surgical applications. For example, the da Vinci Surgical System has been used for prostatectomies, cardiac valve repair and gynecological surgical procedures, and the MAKO System is designed to assist with knee-replacement surgeries. The advantages associated with robotics are improved dexterity, accuracy and repeatability as well as reduced vibration. Furthermore, they can perform tasks in small, constricted places that even the most skilled surgeons cannot and thus the use of robotics is facilitating the growth of minimally invasive surgeries [1].

*Research supported by the Deshpande Center at MIT
Carmen M. Graves is with the Mechanical Engineering Department, Massachusetts Institute of Technology, Cambridge, MA 02139 USA (cmgraves@mit.edu).
Alex Slocum is with the Mechanical Engineering Department, Massachusetts Institute of Technology, Cambridge, MA 02139 USA (e-mail: slocum@mit.edu).
Rajiv Gupta is with the Massachusetts General Hospital, Boston, MA 02114 USA (e-mail: rgupta1@partners.org).
Conor Walsh is with the Harvard School of Engineering and Applied Sciences and the Wyss Institute for Biologically Inspired Engineering at Harvard University, Cambridge, MA 02138 USA (e-mail: walsh@seas.harvard.edu, corresponding author).

The use of medical imaging technologies has also increased in surgical procedures. Ultrasound, Magnetic Resonance Imaging (MRI), fluoroscopy, and Computed Tomography (CT) imaging are all used to image within the body during medical procedures [2]. Imaging allows for improved targeting as it enables the physician to see the position of their instruments with respect to the organs and tissues. In particular, medical imaging is critical during percutaneous procedures that involve the insertion of needles through a single puncture of the skin. In these procedures, such as kidney biopsies and ablations, the radiologist inserts the needle or probe and uses imaging feedback to adjust its position or angle. Robotic devices to assist with these procedures must be compatible with these medical imaging technologies but have been show to improve the targeting accuracy compared to manual interventions. The majority of these systems focus on performing needle orientation and insertion and devices have been demonstrated that are both patient mounted [3-5] and mounted on the CT scanner bed bed [6-8].

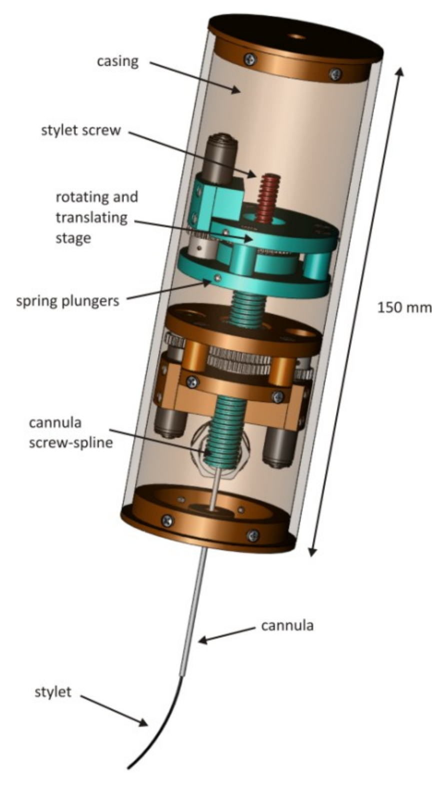

Fig. 1. Illustration of the design of the robotically steerable thermal ablation probe. The cannula is attached to a screw-spline (turquoise) that can be translated and rotated through control of two stepper motors grounded to the casing (brown). The stylet is attached to a screw (red) that can be translated with respect to the screw-spline through control of a motor that is grounded to the screw-spline [9].

Ablation therapy is an example of a minimally invasive percutaneous procedure that is gaining popularity. Thermal or chemical-based ablation therapies can induce cancer cell death within a tumor with an appropriately placed needle. Thermal ablation involves heating or cooling tumor cells in order to destroy them, while ethanol and acetic acid are used as ablative substances in chemical ablation [10]. The most common thermal ablation technique clinically used today is radio-frequency (RF) ablation.

Minimally invasive thermal ablation procedures are inexpensive compared to more invasive open surgeries and result in significantly lower trauma and recovery times. However, the zone of ablation is limited to close to the probe tip. As a result, the focal zone of the ablated tissue may not completely encompass tumors or alternatively, kill a significant amount of healthy tissue, especially in the case of oddly shaped tumors.

Previous work of ours (shown in Fig. 1) proposed using a robotically steerable thermal ablation probe that could reposition the tip of the electrode to multiple adjacent points throughout the tumor [9] to extend the use of thermal ablation. Comprised of plastic and ceramic parts with the majority of the metal components placed outside of the scan plane of the needle, the device was designed for CT-compatibility. The steering mechanism was based on the concept of substantially straightening a pre-curved Nitinol stylet by retracting it into a concentric outer cannula, and re-deploying it at different axial and rotational positions, as also seen in commercially available, passive devices [11, 12], as well as in a robotic hand held device [13]. The drive mechanism is shown in Fig. 2.

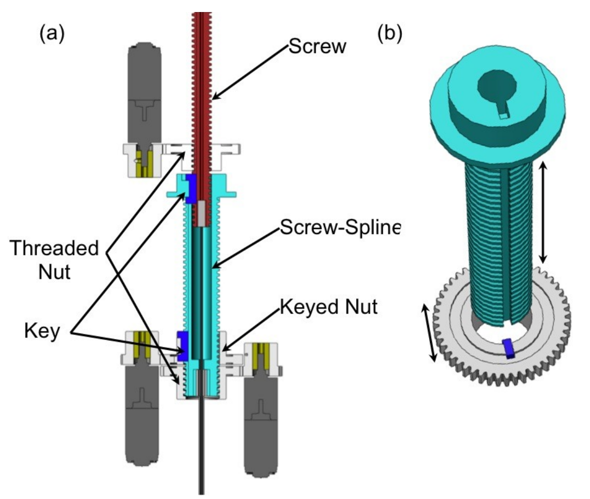

Fig. 2. Previous gear-train design (a) and spline/key interaction (b) [9].

The proximal end of the cannula was attached to the distal end of a screw-spline that enables it to be translated and rotated with respect to the casing. Translation of the stylet relative to the cannula is achieved with a second concentric, nested smaller diameter screw that is constrained to rotate with the cannula.

The previous drive mechanism (shown in Fig. 2(a)) of the robot included two Torlon Acme threaded lead screws with grooves/splines cut into them and running along their length. The screw-spline (cyan) was hollow to allow a nested screw to fit within it. For the screw-spline, a nut with a key (blue) is used to rotationally engage the screw-spline shaft while a threaded nut engages the threads. Similarly, a spline on the screw is matched with another key (blue) on the top of the screw-spline that constrains the screw from rotating while allowing for translation via another threaded nut (Fig. 2(b)).

A. Contribution

In this paper we present design improvements to the drive mechanism for a robotically steerable instrument, outline the forward kinematics of the mechanism and evaluate the system performance in ex-vivo cow liver tissue.

II. Screw-Spline Design and Modeling

To improve manufacturability and assembly of the screw-spline mechanism, an alternative, more robust means was considered for constraining the screw-spline from rotating. The major design goal was to eliminate the need for a spline/key combination for constraining the screw-spline to rotate with the spline nut. The functional requirements for the system were

1. Enable torque to be applied to the shaft
2. Enable free translation of the shaft
3. Capable of mating with a threaded nut for power transmission
4. Enable parts to be inexpensively prototyped
5. Have sufficient strength when manufactured from plastic components

Given these fundamental requirements, a review of other means for constraining rotation and transmitting torque were investigated, finally deciding on a profiled geometry. The screw-spline profile along with the mating "nut" is shown in Fig. 3. As is shown, three flats would be machined onto a shaft that would then be threaded. The flats are just deep enough into the screws to reach the unthreaded portion, and leave sufficient thread to still engage the nuts.

A. Modeling

Fig. 3 illustrates the major design parameters that affect the performance of the mechanism. The gap and contact length are labeled as d and l respectively and the effective radius as r. Fig. 3(b) illustrates the shaft rotated by 5º within the nut.

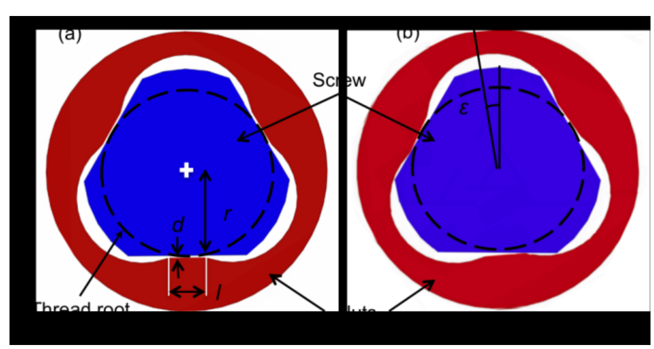

Fig. 3. The profiled screw (blue) and nut (red) shown aligned (a) and rotated (b).

Based on this geometry, a simple model was derived to predict the amount of rotational play for a given gap (due to manufacturing tolerances), contact length and effective radius. The resulting expression is:

$$\cos\varepsilon = \frac{r + \left(l/2\right)\sin\varepsilon}{r + d}, \tag{1}$$

where ε is the angle that describes rotational play from the neutral position. The total angle of play is twice the value of ε. Using MATLAB's Symbolic toolbox, this expression was solved for ε for a range of contact length and gap values and the results are plotted in Fig. 4. To validate the model, various nuts and shafts with varying contact lengths and tolerance gaps were modeled using SolidWorks. In an assembly, the profiled screw was fixed and the gears were rotated in degree increments ranging from 0.1 to 0.5 degrees until a collision was detected using SolidWorks' Move Component and Collision Detection features and the total angle of rotation was recorded. These angles are also included in Fig. 4 as discrete data points. As can be seen, the data from SolidWorks closely matched the analytical model.

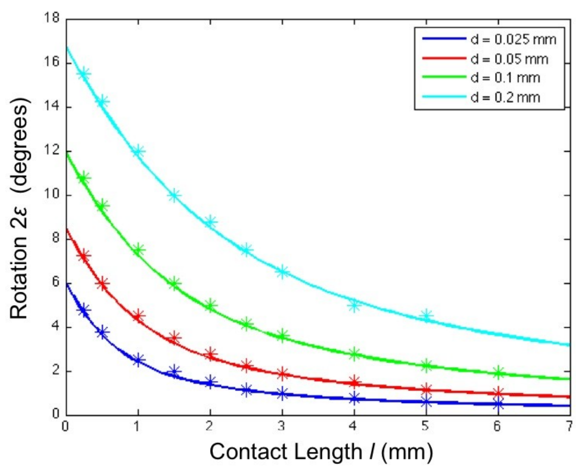

Fig. 4. Maximum backlash between profiled nut and screw as a function of contact length and different tolerance gaps calculated using a geometric model and SolidWorks.

Thus it is the small tolerance gap and the length of the contact portion that have an effect on the backlash between the nut and the screw. After modeling the behavior of the nuts as contact length and tolerance gaps, a final geometry with a contact length of approximately 6.5 mm was decided upon. Using this geometry, the analytical model predicted that the angular play between the screw and the nut would be about 2 degrees which was deemed acceptable for the target application.

B. Embedded Fiducial Markers for Registration

A fiducial point-based registration method was used with markers embedded in the casing, as shown in Fig. 5. The markers are aligned in a spiral pattern, away from the metallic parts of the robot, so as to minimize the chance of poor registration due to artifacts. Six markers were used, and the distance between each marker was chosen to be distinct to aid with the registration.

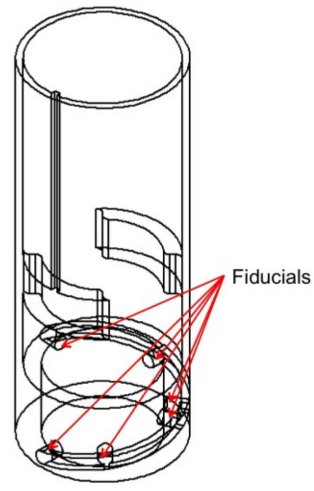

Fig. 5. Six markers are imbedded in the robot casing in a pattern in which the distance between any two markers are different (dimensions in mm). The robot is attached to the shelves within the casing.

C. Manufacturing

Each flat on the threaded rod was in contact with a flat on the nut. This profile was chosen to be relatively easy to machine. An intersecting bolt circle makes up the three lobes, and minimal machining prepares the corners between the hole centers to match up with the flats on the screws. The prototyped parts can be seen in Fig. 6.

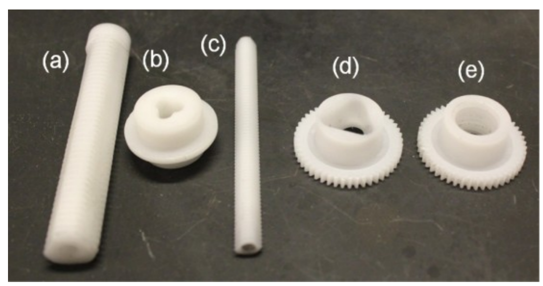

Fig. 6. The fabricated parts: (a) screw-spline; (b) profiled top; (c) screw; (d) profiled nut; and (e) threaded screw-spline nut.

This design ensured minimal constraint and ensured there was no pressure on the threads, while being robust to misalignment and jamming. The transmission with the newly prototyped parts is shown in Fig. 7.

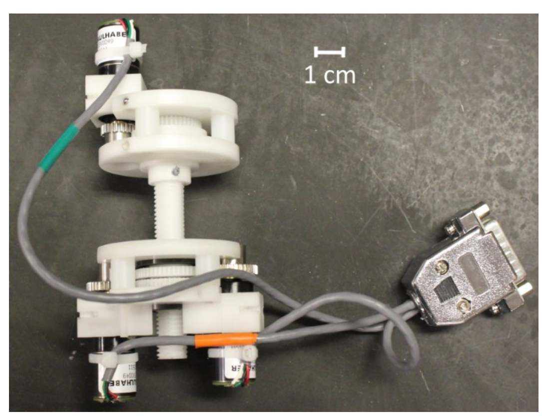

Fig. 7. The electromechanical portion of the robot.

D. Assembly

A pre-curved hollow stylet with an outer diameter (OD) of 1.25 mm, an inner diameter (ID) of 1.00 mm, and a radius of curvature of about 40mm was manufactured using the process described in [14]. A straight cannula with ID 1.5 mm and OD of 2.0 mm was selected to be used with this stylet. The hollow pre-curved stylet allows for a thin RF electrode or fluid to be deployed through it, thus maximizing the flexibility of the system for testing purposes. The drive mechanism was housed in a case that covers all of the motors and moving parts. Only the wires used to control the robot as well as the cannula and stylet extend from the casing, as shown in Fig. 8.

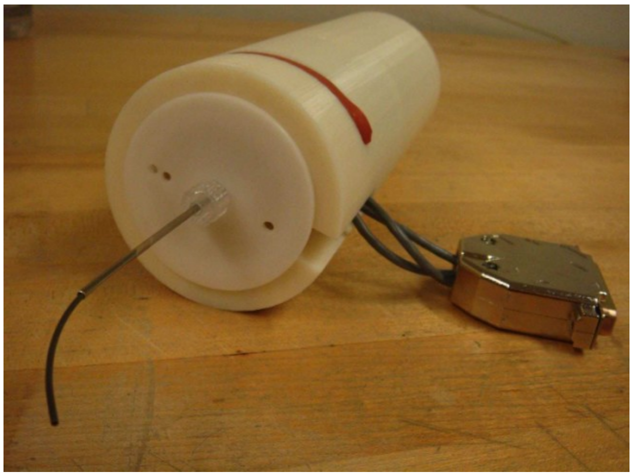

Fig. 8. The robot fully assembled within the casing.

III. Mechanism Kinematics

The robot is intended to be controlled via an image-based interface implemented with 3D Slicer. Specifically, the ProstateNav module was modified to account for a different set of robot kinematics and registration method.

A. Forward Kinematics

In order to predict the tip location, a kinematic model based on a series of homogeneous transformation matrices (HTM) was developed. The locations of the coordinate systems (CSs) are shown in Fig. 9, with the origin labeled. The locations of the coordinate systems relative to each other are a function of the actuation inputs and expressions derived from characterization of the needle steering mechanism. The first HTM is

$$^{0}HTM_{1} = \begin{bmatrix} \cos\theta_{z} & -\sin\theta_{z} & 0 & 0 \\ \sin\theta_{z} & \cos\theta_{z} & 0 & 0 \\ 0 & 0 & 1 & z_{c} \\ 0 & 0 & 0 & 1 \end{bmatrix}, \quad (2)$$

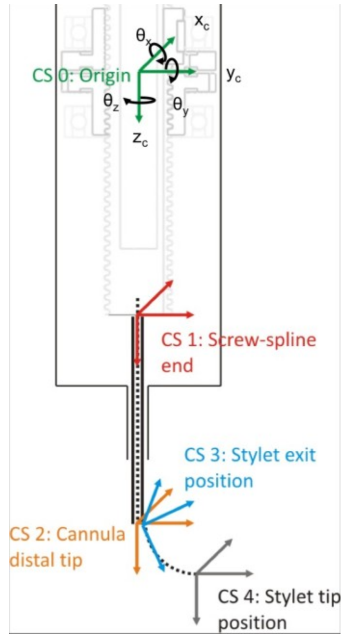

Fig. 9. Locations of coordinate systems chosen for the kinematic model.

where θ_z and z_c are the angular and axial positions of the screw-spline respectively. The cannula takes a slightly curved shape when the stylet is inside it. This results in an angular and an additional translational shift between the two coordinate systems. The tip of the cannula relative to its attachment to the screw-spine is defined by $^{1}HTM_{2}$:

$$^{1}HTM_{2} = \begin{bmatrix} 1 & 0 & 0 & 0 \\ 0 & \cos\theta_{x} & -\sin\theta_{x} & R(1-\cos\theta_{x}) \\ 0 & \sin\theta_{x} & \cos\theta_{x} & l-(l_{0}-R\sin\theta_{x}) \\ 0 & 0 & 0 & 1 \end{bmatrix}. \quad (3)$$

θ_x, the angular displacement of the tip, is equal to the included angle of the curved cannula which is l_0/R where l_0 is the overlap length between the curved stylet and straight cannula, and R is the radius of curvature of the stylet in its undeflected state. The stylet exits the cannula at an incident angle. $^{2}HTM_{3}$ relates these two coordinate systems and is given by

$$^{2}HTM_{3} = \begin{bmatrix} 1 & 0 & 0 & 0 \\ 0 & \cos\theta_{x} & -\sin\theta_{x} & 0 \\ 0 & \sin\theta_{x} & \cos\theta_{x} & 0 \\ 0 & 0 & 0 & 1 \end{bmatrix}, \quad (4)$$

where θ_x in this case is the value obtained from

$$\theta_{x} = \frac{\pi}{2} - \sin^{-1}\left(1 - \frac{d_{c}-d_{s}}{R}\right). \quad (5)$$

where d_c is the cannula ID, d_s is the stylet OD. Finally, $^{3}HTM_{4}$ relates the stylet tip position relative to the tip of the cannula. The y and z positions are a function of the command for stylet screw deployment from the cannula, z_s, as well as the radius of curvature.

$$
{}^{3}HTM_{4} = \begin{bmatrix} 1 & 0 & 0 & 0 \\ 0 & 1 & 0 & R\left(1-\cos\left(\frac{z_s}{R}\right)\right) \\ 0 & 0 & 1 & R\sin\left(\frac{z_s}{R}\right) \\ 0 & 0 & 0 & 1 \end{bmatrix} \tag{6}
$$

The overall transformation is a multiplication of all of the individual HTMs and relates the origin of the robot (set at the midpoint of the two nuts as shown) to the distal tip of the stylet.

$$
{}^{0}HTM_{4} = {}^{0}HTM_{1}\,{}^{1}HTM_{2}\,{}^{2}HTM_{3}\,{}^{3}HTM_{4} \tag{7}
$$

However, it should be noted that there are a number of limitations to this model. The model does not account for the added deflection of the cannula as it is inserted through tissue (due to its slightly curved shape and resultant asymmetric forces on it). Furthermore, the stylet will also deviate from its natural shape as it is inserted into tissue due to a tangential cutting force at its tip and thus no longer have a constant radius of curvature. The amount of deflection will be a function of the stylet geometry (radius of curvature and stylet diameter).

IV. System Evaluation

In order to gain information pertaining to the performance of the drive mechanism and how the stylet deflects in tissue, testing was done by inserting the needles into ex vivo tissue samples. A Definition Flash CT scanner (Siemens Medical Solutions, Erlangen, Germany) at the Massachusetts General Hospital was used to visualize the stylet after it was deployed into the tissue by the mechanism in 600 µm slices. The rig suspending the robot was placed inside the CT scanner bore above a bovine liver sample as shown in Fig. 10.

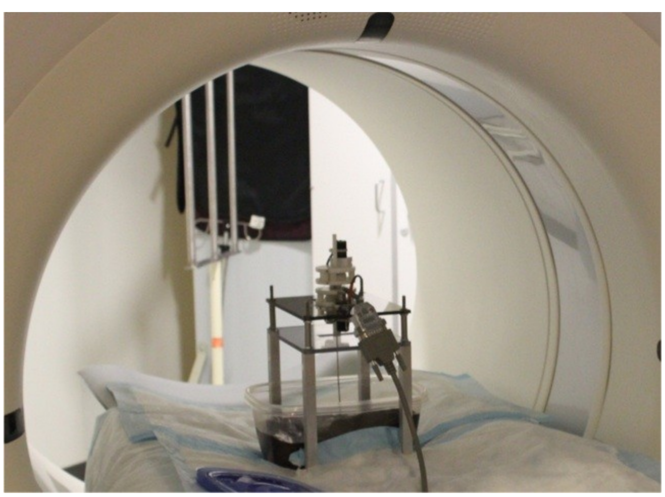

Fig. 10. CT scanning test setup used to view stylet within the ex vivo tissue sample.

Before each test, a level was used to ensure that the rig was horizontal with respect to the scanner, and the stylet was oriented perpendicular to the scan planes. The cannula was inserted into the tissue and the stylet was deployed before the rig was moved into the scan area and imaging was performed. The images taken by the CT scanner were saved as DICOM (Digital Imaging and Communications in Medicine) files. An example image is shown in Fig. 11.

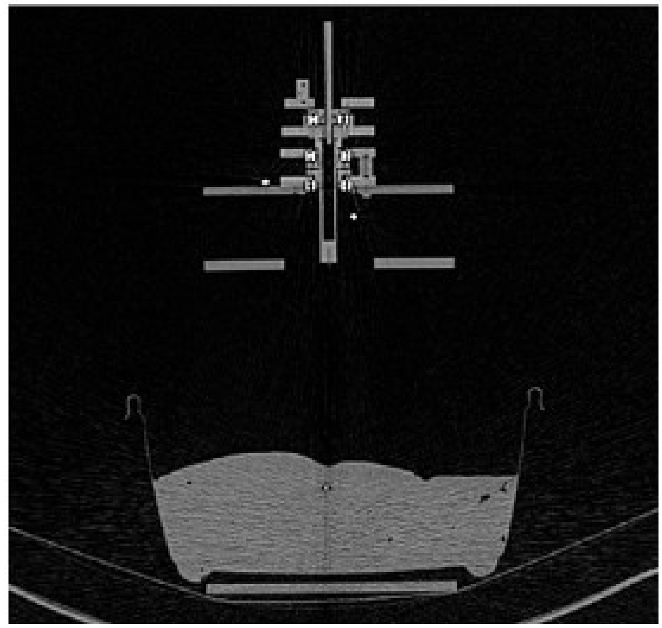

Fig. 11. Cross-sectional CT image of the steerable needle robot with stylet inserted in ex vivo liver tissue.

Four insertion tests were performed using 0.635 mm and 0.838 mm diameter stylets with radii of curvatures of 10 mm and 40 mm. In order to characterize the curvature of the stylet, the stylet tip location was identified and recorded in consecutive images as seen in Fig. 12.

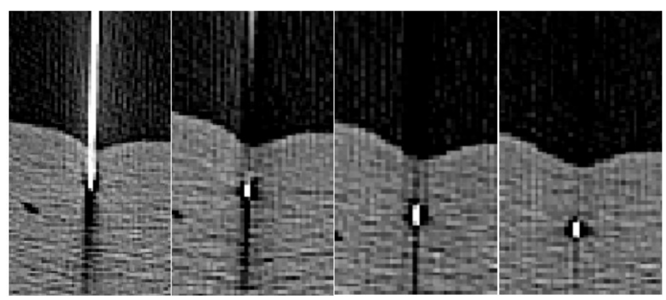

Fig. 12. Consecutive cross-sections of the stylet allow for visualization of the stylet curve.

A MATLAB script was used to cycle through all of the DICOM images acquired from the CT scanner. While cycling through the images, the user clicks on the position of the stylet. When the crosshairs are in the position, clicking would place a dot on the bottom most portion of the cross-section of the stylet seen in the image.

The points of the stylet were recorded and plotted in 3D. This data was then compared to predictions of the path of the stylet in tissue found using a model based on the HTMs. The data recorded from the DICOM images along with that from the model are compared in Fig. 13.

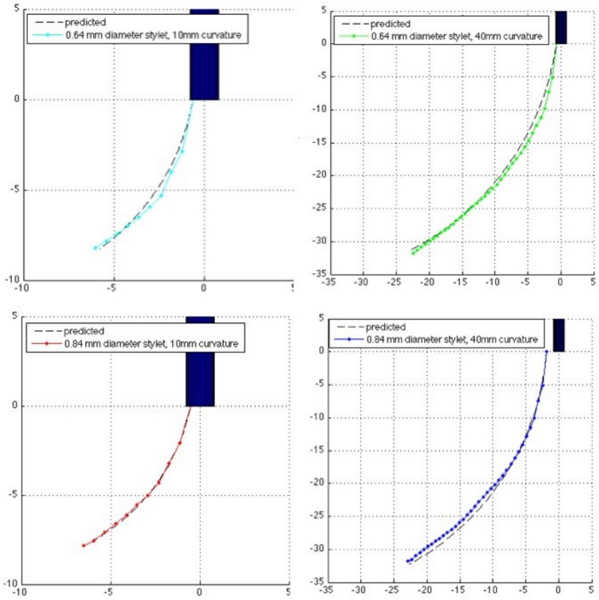

Fig. 13. Recorded (colored) and predicted (---) stylet curvatures for stylets of diameter 0.635 mm (top) and 0.838 mm (bottom) with radii of curvature of about 10 mm (left) and 40 mm (right).

The end points of the stylets can be determined from the data collected. These points are compared to those predicted by the forward kinematic model. The errors between the stylet end points and the predicted end points are listed in Table 1. The end-point targeting error observed was consistently less than 2 mm, providing a preliminary demonstration of the successful operation of the drive mechanism for repositioning a stylet in ex-vivo tissue.

TABLE I. END POINT ERRORS

Stylet Diameter (mm)	Curvature Radius (mm) [14]	Stylet Deployment (mm)	End Point Error (mm)
0.635	13.1	10	0.4
0.635	42.2	40	1.5
0.838	11.2	10	0.3
0.838	40.3	40	1.7

V. CONCLUSION AND FUTURE WORK

The goal of this paper was to outline the design, demonstration and evaluation of a robustly functioning drive mechanism for a robotically steerable medical instrument. The results showed that the prototype performs reliably and the design and evaluation tools can easily be adapted for other applications.

A modified screw-spline mechanism was created using a profiled shaft and matching nut rather than spline and key. This mechanism can be easily and cheaply constructed from plastic components, and can be manufactured at a larger scale by injection molding and with a minimal number of parts. A model based on the geometry of the screw and nut was developed to characterize the performance of the profile mechanism. This model was validated using SolidWorks and the prototyped screw-spline and nut had an angular play of approximately 2.25 degrees that corresponds well with the value of 2 degrees predicted by the mathematical model.

The forward kinematics for the prototype were derived using homogenous transformation matrixes that were used to predict the stylet tip position based on actuator position inputs. DICOM images of the stylet in ex-vivo liver tissue were taken in the CT scanner, which were then analyzed. The stylet paths were extracted from the data, and compared to predicted results. The model was consistently within 2 mm of the actual stylet tip position. The major result of this paper is a robustly functioning, accurate drive mechanism for a robotically steered needle that can now be integrated with a thermal ablation probe.

ACKNOWLEDGMENT

We would like to acknowledge the contribution of Jan Harms on the MATLAB script used to record the x,y,z coordinates of the stylet through a stack of CT images. This work was supported by the Deshpande Center for Technological Innovation at the Massachusetts Institute of Technology.

REFERENCES

[1] D. B. Camarillo, T. M. Krummel, J. K. Salisbury Jr., "Robotic technology in surgery: Past, present, and future," *American Journal of Surgery*, vol. 188, supplement 4, pp. 2S-15S, 2004.

[2] S. N. Goldberg, C. J. Grassi, J. F. Cardella, et al., "Image-guided Tumor Ablation: Standardization of Terminology and Reporting Criteria," *Radiology*, vol. 235, pp. 728-739, 2005.

[3] E. Taillant*, et al.*, "CT and MR Compatible Light Puncture Robot: Architectural Design and First Experiments," *MICCAI 2004*, pp. 145-152, 2004.

[4] B. Maurin*, et al.*, "A robotized positioning platform guided by computed tomography: practical issues and evaluation," *IEEE: ICRA 2006*, pp. 251-256, 2006.

[5] C. Walsh*, et al.*, "A Patient-Mounted, Telerobotic Tool for CT-Guided Percutaneous Interventions," *ASME Journal of Medical Devices,* vol. In Press, 2008.

[6] A. Bzostek*, et al.*, "A Testbed System for Robotically Assisted Percutaneous Pattern Therapy," *MICCAI'99,* vol. 1679, pp. 1098-1107, 1999.

[7] D. Stoianovici*, et al.*, "AcuBot: a robot for radiological interventions," *Robotics and Automation, IEEE Trans. on,* vol. 19, pp. 927-930, 2003.

[8] M. Rasmus*, et al.*, "Preliminary clinical results with the MRI-compatible guiding system INNOMOTION," *Int J CARS* vol. 2 pp. S138-S145, 2007.

[9] C. Walsh, J. Franklin, A. Slocum, R. Gupta. *Design of a Telerobot for Percutaneous Instrument Distal Tip Repositioning* (paper, poster and oral presentation), IEEE EMBC Conference, August 30 – September 3, 2011.

[10] M. Ahmed, C. Brace, F. Lee, S. Goldberg. "Principles of and Advances in Percutaneous Ablation." *Radiology*, vol. 258: no. 2., pp. 351-69, February 2011.

[11] R. L. Pakter and E. M. Morris, "Hollow, curved, superlastic medical needle," vol. US Patent No. 6,592,559 B1.

[12] W. R. Daum, "Deflectable Needle Assembly," US Patent No. 6,572,593.

[13] S. Okazawa, *et al.*, "Hand-Held Steerable Needle Device." *IEEE/ASME Transactions on Mechatronics*, vol. 10: no. 3, pp. 285-296, 2005.

[14] C. Walsh, J. Franklin, A. Slocum, R. Gupta. *Characterization of Pre-curved Needles for Use in Distal Tip Manipulation Mechanisms* (paper, poster and oral presentation), ASME Design of Medical Devices Conference, April 13-15, 2010.